1-1-2004

Time-reversal imaging with multiple signal classification considering multiple scattering, between the targets

Fred K. Gruber
University of Central Florida

Edwim A. Marengo

Anthony J. Devaney

Recommended Citation

University of
Central Florida

STARS
Showcase of Text, Archives, Research & Scholarship

Time-reversal imaging with multiple signal classification considering multiple scattering between the targets

Fred K. Gruber, Edwin A. Marengo, and Anthony J. Devaney

ARTICLES YOU MAY BE INTERESTED IN

Time-reversal-based imaging and inverse scattering of multiply scattering point targets
The Journal of the Acoustical Society of America **118**, 3129 (2005); https://doi.org/10.1121/1.2042987

Transmission mode time-reversal super-resolution imaging
The Journal of the Acoustical Society of America **113**, 2742 (2003); https://doi.org/10.1121/1.1566975

Experimental subwavelength localization of scatterers by decomposition of the time reversal operator interpreted as a covariance matrix
The Journal of the Acoustical Society of America **114**, 235 (2003); https://doi.org/10.1121/1.1568759

Decomposition of the time reversal operator: Detection and selective focusing on two scatterers
The Journal of the Acoustical Society of America **99**, 2067 (1996); https://doi.org/10.1121/1.415393

Time-reversal multiple signal classification in case of noise: A phase-coherent approach
The Journal of the Acoustical Society of America **130**, 2024 (2011); https://doi.org/10.1121/1.3626526

The iterative time reversal process: Analysis of the convergence
The Journal of the Acoustical Society of America **97**, 62 (1995); https://doi.org/10.1121/1.412285

Time-reversal imaging with multiple signal classification considering multiple scattering between the targets

Fred K. Gruber[a)]

Department of Industrial Engineering and Management Systems, University of Central Florida, Orlando, Florida 32816 and Department of Electrical Engineering, Technological University of Panama, Apartado 6-2894, Panama City, Panama

Edwin A. Marengo

Department of Electrical and Computer Engineering, Northeastern University, Boston, Massachusetts 02115 and Department of Electrical Engineering, Technological University of Panama, Apartado 6-2894, Panama City, Panama

Anthony J. Devaney

Department of Electrical and Computer Engineering, Northeastern University, Boston, Massachusetts 02115

The time-reversal imaging with multiple signal classification method for the location of point targets developed within the framework of the Born approximation in Lehman and Devaney [''Transmission mode time-reversal super-resolution imaging,'' J. Acoust. Soc. Am. **113**, 2742–2753 (2003)] is generalized to incorporate multiple scattering between the targets. It is shown how the same method can be used in the location of point targets even if there is multiple scattering between them. On the other hand, both the conventional images and the calculated values of the target scattering amplitudes are scattering model-dependent. © *2004 Acoustical Society of America.* [DOI: 10.1121/1.1738451]

I. INTRODUCTION

Time-reversal (TR) methods have been of interest for a number of years, with applications ranging from medicine, to communications, to radar, and to imaging in general.[1–6] A particular TR technique that has received much attention is a TR imaging with multiple signal classification (MUSIC) method for the location of point targets (whose size is much smaller than the wavelength) established first for coincident arrays,[7] and elaborated further in a recent generalization to noncoincident arrays and nonreciprocal media[8] and a recent super-resolution analysis based on real data.[9] This TR imaging with MUSIC method blends the original TR focusing[10,11] with signal subspace methods, in particular, with the MUSIC estimation technique. In its basic form the method is designed to deduce the location of point targets embedded in a known background medium from knowledge of the measured multistatic response matrix K of an acoustic or electromagnetic transceiver array actively interrogating the targets. It provides a powerful approach for locating targets in both homogeneous and heterogeneous backgrounds, especially in cases of closely spaced targets and/or very sparse transceiver arrays. However, these developments are based on the (distorted wave) Born approximation. The present letter addresses the corresponding generalization if there is non-negligible multiple scattering between the targets.

II. GENERALIZATION INCLUDING MULTIPLE SCATTERING BETWEEN THE TARGETS

We consider an array of N time-harmonic transceivers located at the space points $\mathbf{R}_j$, for $j=1,2,\ldots,N$. Each transceiver can radiate into a reciprocal propagating medium in which are embedded $M<N$ point targets having unknown positions $\mathbf{X}_m$ and unknown target scattering amplitudes τ_m, for $m=1,2,\ldots,M$. For simplicity, we model the field radiated by the jth transceiver as the scalar field $G(\mathbf{r},\mathbf{R}_j)e_j$ where $G(\mathbf{r},\mathbf{r}')$ is the Green function of the propagating medium (in principle, the ''medium'' can include the transceivers themselves so inter-transceiver coupling can be built in this Green function) and e_j is the excitation applied to the transceiver.

A. Review of the TR imaging with MUSIC method

Under the Born approximation the TR imaging with MUSIC method is based on the fact that, for fewer targets than transceivers, the space $\mathcal{C}^N$ of voltage vectors applied to the N-transceiver array can be decomposed into the direct sum $\mathcal{C}^N=\mathcal{S}\oplus\mathcal{N}$, where the signal subspace $\mathcal{S}$ is orthogonal to the noise subspace $\mathcal{N}$, where $\mathcal{S}$ is spanned by the principal eigenvectors μ_i of the TR matrix $T=K^{\dagger}K$ (where $\dagger$ denotes the adjoint) having nonzero eigenvalues (if there are $M<N$ targets then there are at most M such eigenvalues indexed from 1 to M) whereas $\mathcal{N}$ is spanned by the eigenvectors μ_i of T having zero eigenvalues (if there are $M<N$ targets then there are at least $N-M$ such eigenvalues indexed from $M+1$ to N). The key result is that the TR matrix T is essentially a projection operator onto the space spanned by the complex conjugates g_m^* of the Green function vectors defined

a)Electronic mail: fgruber@mail.ucf.edu

as $g_m = [G(\mathbf{R}_1, \mathbf{X}_m), G(\mathbf{R}_2, \mathbf{X}_m), \ldots, G(\mathbf{R}_N, \mathbf{X}_m)]^t$ where t denotes the transpose, so that in general the principal eigenvectors of T are linear combinations of the g_m^*'s. It follows from this and the orthogonality of the signal and noise subspaces that the target locations must correspond to the poles in the MUSIC pseudospectrum

$$D(\mathbf{X}_p) = \frac{1}{\Sigma_{i=M+1}^{N} |\langle \mu_i^* | g_p \rangle|^2}, \tag{1}$$

where for all $i = M+1, M+2, \ldots, N$ the inner product $\langle \mu_i^* | g_p \rangle \equiv \mu_i^t g_p = 0$ whenever $\mathbf{X}_p$ is the actual location of one of the targets.

B. Our main results

Essentially, what we show next is that not only for the Born-approximated model but also for the more general case when there is multiple scattering between the targets the TR matrix T is a projection operator onto the space spanned by the complex conjugates g_m^* of the Green function vectors g_m so that in general the principal eigenvectors of T are linear combinations of the g_m^*'s. It follows that the same TR imaging with MUSIC method described in connection with Eq. (1) can be used in the location of point targets even if there is multiple scattering between them. On the other hand, both the conventional TR images,[10,11] corresponding to back-propagations of the principal eigenvectors, and the calculated values of the target scattering amplitudes are scattering model-dependent.

C. Formulation

The exact scattered field $\psi_j^{(s)}(\mathbf{r})$ at position $\mathbf{r}$ due to the excitation of the jth transceiver alone can be expressed as the Newman series

$$\psi_j^{(s)}(\mathbf{r}) = \sum_{m=1}^{M} G(\mathbf{r}, \mathbf{X}_m) \tau_m G(\mathbf{X}_m, \mathbf{R}_j) e_j$$

$$+ \sum_{m=1}^{M} \sum_{m'=1}^{M} G(\mathbf{r}, \mathbf{X}_m) \tau_m G(\mathbf{X}_m, \mathbf{X}_{m'})$$

$$\times \tau_{m'} G(\mathbf{X}_{m'}, \mathbf{R}_j)(1 - \delta_{m,m'}) e_j$$

$$+ \sum_{m=1}^{M} \sum_{m'=1}^{M} \sum_{m''=1}^{M} G(\mathbf{r}, \mathbf{X}_m) \tau_m G(\mathbf{X}_m, \mathbf{X}_{m'})$$

$$\times \tau_{m'} G(\mathbf{X}_{m'}, \mathbf{X}_{m''}) \tau_{m''} G(\mathbf{X}_{m''}, \mathbf{R}_j)$$

$$\times (1 - \delta_{m,m'})(1 - \delta_{m',m''}) e_j + \cdots, \tag{2}$$

where $\delta_{..}$ denotes the Kronecker delta. The first sum in Eq. (2) corresponds to the Born-approximated case, the second sum corresponds to the second-order scattering contribution, and so on.

The multistatic response matrix K, whose entry $K_{l,j}$ is defined as the value of the scattered field detected at the lth transceiver (in receive mode) due to the unit excitation at the jth transceiver (in transmit mode), can be shown from Eq. (2) to be given by (see also Borcea et al.[12])

$$K = \sum_{m=1}^{M} g_m \tau_m \Lambda_m^t, \tag{3}$$

where

$$\Lambda_m^t = g_m^t + \sum_{m'=1}^{M} G(\mathbf{X}_m, \mathbf{X}_{m'}) \tau_{m'}(1 - \delta_{m,m'}) g_{m'}^t$$

$$+ \sum_{m'=1}^{M} \sum_{m''=1}^{M} G(\mathbf{X}_m, \mathbf{X}_{m'}) \tau_{m'} G(\mathbf{X}_{m'}, \mathbf{X}_{m''}) \tau_{m''}(1$$

$$- \delta_{m,m'})(1 - \delta_{m',m''}) g_{m''}^t + \cdots \tag{4}$$

(the approximation $\Lambda_m^t \simeq g_m^t$ yields the multistatic response matrix in the Born-approximated model). It follows from Eq. (3) that the TR matrix $T = K^\dagger K = K^* K$, where the second equality follows from reciprocity, can be expressed as

$$T = \sum_{m=1}^{M} \sum_{m_0=1}^{M} g_m^* \tau_m^* \langle \Lambda_m | g_{m_0} \rangle \tau_{m_0} \Lambda_{m_0}^t. \tag{5}$$

Put in this form, the TR matrix T is identified to be under the most general multiple scattering conditions a projection operator onto the space spanned by the complex conjugates g_m^* of the Green function vectors g_m so that in general the principal eigenvectors of T are linear combinations of the g_m^*'s, with the music pseudospectrum $D(\mathbf{X}_p)$ in Eq. (1) having poles at the locations of the targets, as desired. We illustrate this generalization next for a few canonical examples based on the free space Green function in two-dimensional space.

D. TR imaging with MUSIC in the second-order scattering case

In the following computer illustrations we consider the second-order scattering approximation of the preceding general theory. Our main goal is to show that despite the presence of non-negligible second-order scattering the TR imaging with MUSIC method works well in predicting the target locations. We will introduce a normalized quantity, to be referred to as "the second-order scattering contribution factor," and defined as $\eta = |\text{Tr}[(K_{2\text{nd}} - K_{\text{Born}})^*(K_{2\text{nd}} - K_{\text{Born}})]|/\text{Tr}(T_{\text{Born}})$, where Tr denotes the trace, K_{Born} and T_{Born} are the multistatic response matrix and the TR matrix, respectively, assuming the Born approximation, and $K_{2\text{nd}}$ is the multistatic response matrix for a more general second-order scattering model, as a way to quantify the global effect of the second-order scattering contribution relative to that of the first-order scattering term alone as seen by the array in receive mode. This factor measures the deviation of the data matrix (K), as determined by the energy norm or inner product metric, relative to the purely Born-approximated vector, due to the second-order scattering contribution.

Figures 1 and 2 show plots in gray color map of the MUSIC pseudospectra under a second-order scattering model for a number of transceiver and target configurations. Next to each MUSIC pseudospectrum plot we have provided another plot showing the corresponding simulation geometry where the transceiver locations are indicated with triangles while the target locations are indicated with asterisks. All dimensions are relative to the wavelength λ (which equals

J. Acoust. Soc. Am., Vol. 115, No. 6, June 2004

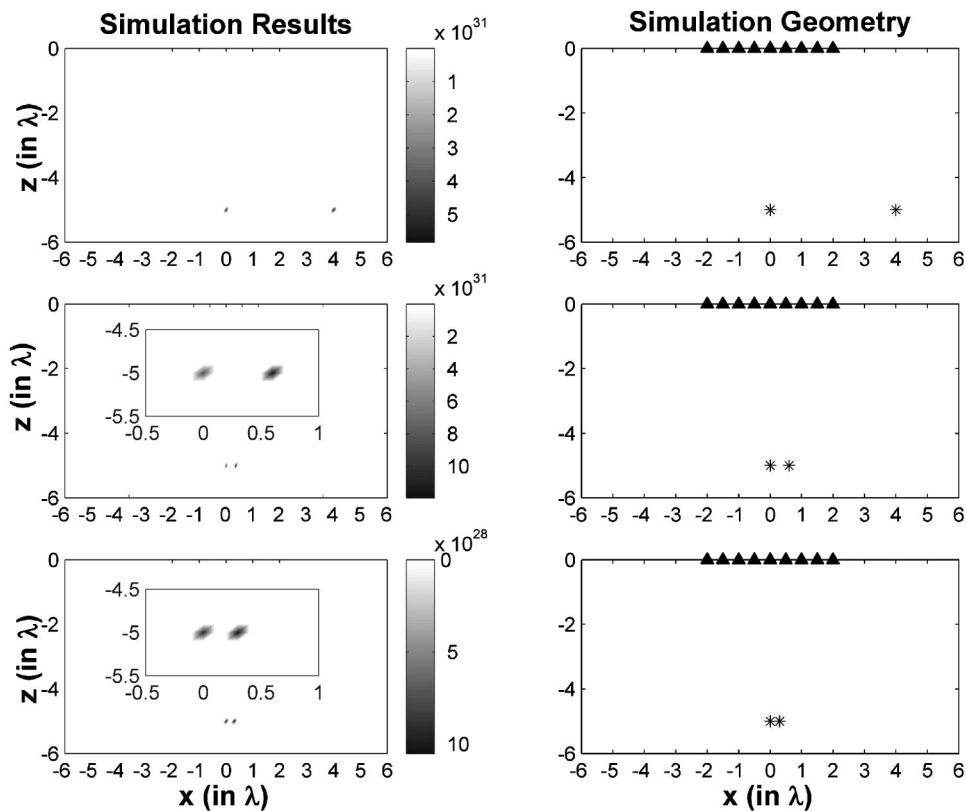Gruber et al.: Time-reversal imaging   3043

FIG. 1. Reconstructed image with an inverse gray color map for the second-order scattering simulation pseudospectrum for a two target configuration. Three target separations are shown: 4λ (top), 0.6λ (middle), and 0.3λ (bottom). A linear scale was used for the horizontal and vertical axes.

1), and all targets have unit scattering amplitude. The plot in Fig. 1 illustrates the super-resolution capabilities of the technique[9] since even for a target separation as small as 0.3λ the target locations remain sharply resolved [the method was found to work for yet smaller target separations, in particular, 0.1λ (results not shown)]. For the 0.6λ and 4λ target separation cases the second-order contribution factor is not very strong ($\eta=0.17$ and $\eta=0.03$, respectively). However, for the 0.3λ and 0.1λ target separation cases, the second-order contribution factor is $\eta=0.33$ and $\eta=0.89$, respectively.
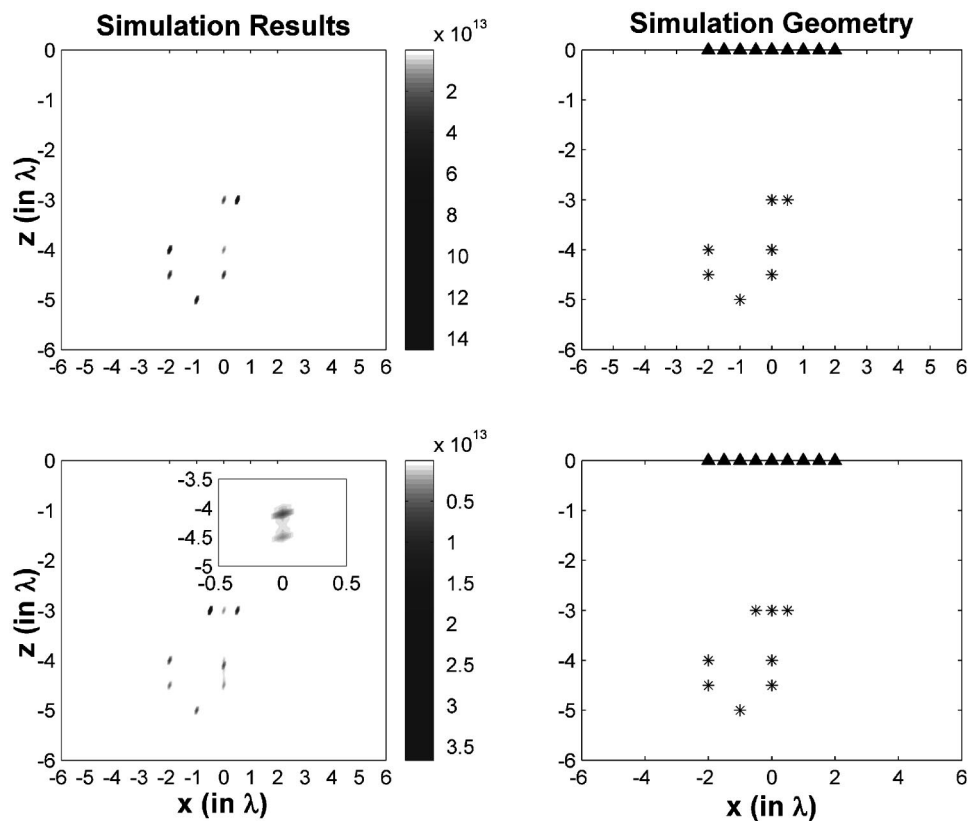

FIG. 2. Reconstructed image with an inverse gray color map for the second-order scattering simulation pseudospectrum for 7 and 8 targets in a *J* conformation. A linear scale was used for the horizontal and vertical axes.

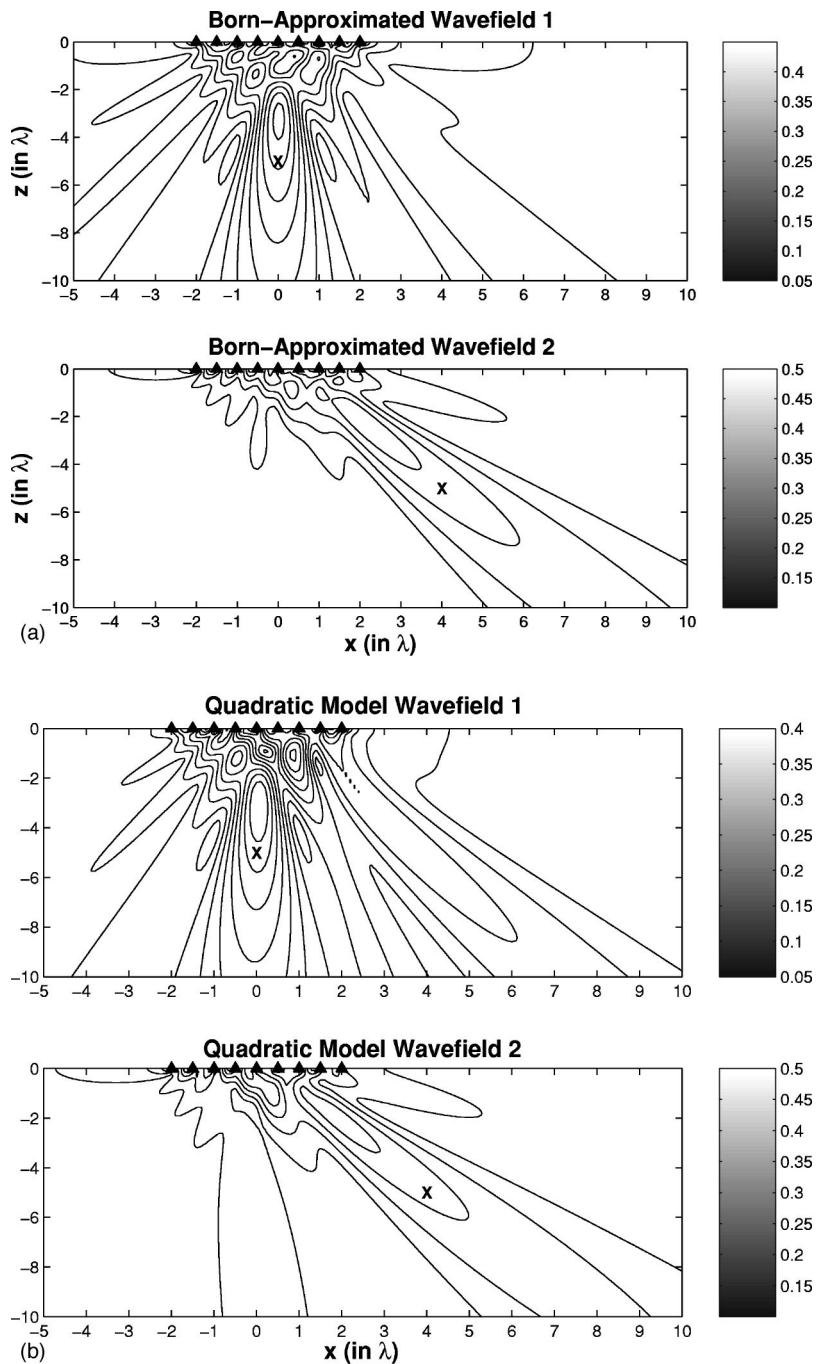Gruber *et al.*: Time-reversal imaging

FIG. 3. (a) Conventional, backpropagated images of the two principal eigenvectors corresponding to the 4λ target separation geometry in Fig. 1. Results for the Born-approximated model. A linear scale was used for the horizontal and vertical axes. (b) Corresponding results for the second order scattering model.

This means that in the 0.3λ target separation configuration the amount of additional signal due to the presence of second-order scattering is of the order of the Born-approximated signal alone as perceived by the array in receive mode. In the 0.1λ target separation case the presence of second-order scattering is even more dominant. Yet the TR imaging with MUSIC was found to succeed in determining the target locations. More complicated seven and eight target configurations forming a J and having significant second-order scattering contribution factors of $\eta=0.31$ and $\eta=0.30$, respectively, are considered in Fig. 2. The method works well in predicting the target locations but for the eight target case the prediction for one of the target locations, in particular, the one at the plot coordinates $(0,-4\lambda)$, has a slight error which we attribute to computational sensitivity

under reduced noise subspace conditions (in this extreme case when $M=8$ and $N=9$ the noise subspace has a single eigenvector).

E. Time-reversed images: Born-approximated versus second-order scattering cases

The field radiated by the array due to excitation with an arbitrary voltage vector is $\psi(\mathbf{r})=\Sigma_{j=1}^{N}G(\mathbf{r},\mathbf{R}_j)e_j$. In the original TR focusing one obtains backpropagated images $\psi(\mathbf{r})$ of the targets by replacing the arbitrary input voltage vectors in this expression with the principal eigenvectors of the TR matrix. If there is no second-order scattering between the targets then the principal eigenvectors are precisely the complex conjugates of the Green function vectors and each
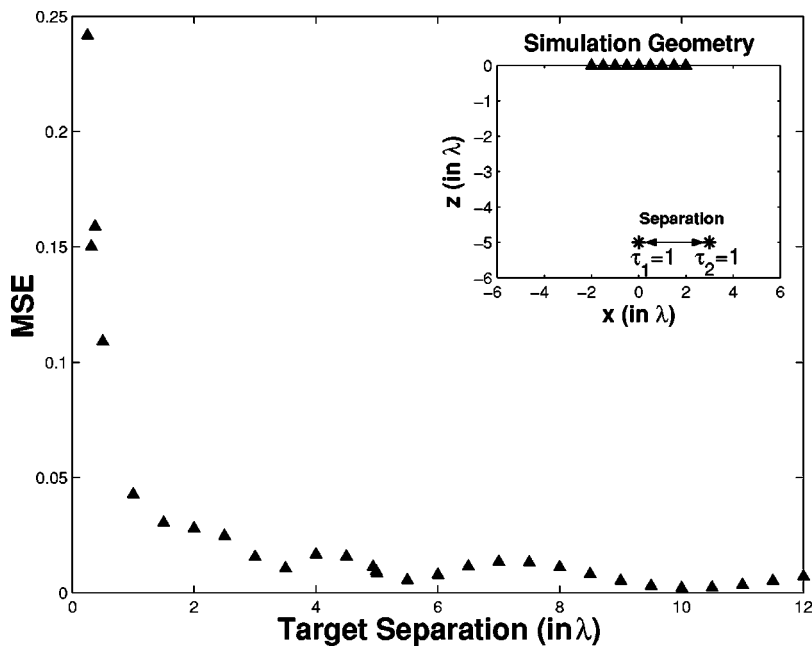
FIG. 4. MSE in scattering amplitude estimation, incurred if one uses the Born-approximated model instead of the more exact second-order scattering model, as a function of target separation for the general two target configuration used in Fig. 1.

one of them is associated with (focuses on) a particular target. Consequently, as shown in Fig. 3(a), corresponding to the 4λ target separation case in Fig. 1, in the Born-approximated case each "eigenimage" focuses on a particular, corresponding target (in the plots we have superimposed an X in the location of the corresponding target). On the other hand, if there is second-order scattering between the targets, then the principal eigenvectors become linear combinations of the complex conjugates of the Green function vectors so that each eigenimage focuses in general on more than one target (this is somehow similar to the results in Ref. 11 for non-well-resolved targets). Figure 3(b) illustrates this effect for the second-order scattering case where each eigenimage is seen to focus on *both* targets.

F. Target scattering amplitudes: Born-approximated versus second-order scattering cases

In the general case including multiple scattering considered here, once the target locations are determined from the poles in the MUSIC pseudospectrum one can compute the unknown target scattering amplitudes by substituting the values of these locations in Eq. (3) and solving the resulting system of equations. In general, such computed values will depend on the scattering model employed, being more exact for a more exact scattering model. To illustrate this let us assume that in reality the response obeys a second-order scattering model. If we try to determine the scattering amplitudes considering a Born-approximated model then we will have model-induced errors. Figure 4 shows, again for the geometry in Fig. 1, the mean square error (MSE) in the estimation of the scattering amplitudes (as measured relative to the more exact second-order scattering model) as a function of target separation. The errors are significant (relative to the value $\tau_1 = \tau_2 = 1$) for targets in close proximity, as expected (second-order scattering becomes then more prevalent).

III. CONCLUSION

In this letter we showed that the TR imaging with MUSIC method can be used to locate point targets not only in the usual framework of the Born approximation but also in more general nonlinear scattering frameworks where there is multiple scattering between the targets. This finding is important toward practical implementations of the TR technique facing multiple scattering effects. The super-resolution results of a previous paper[9] can now be better characterized theoretically in the multiple scattering regime. They were also corroborated numerically for second-order scattering (see Fig. 1). The method was found to work well even for a large number of targets relative to the number of transceivers (see Fig. 2) although slight numerical challenges may arise as the number of targets approaches the number of transceivers (see the zooming part of Fig. 2). We showed how both the conventional, backpropagated images of the principal eigenvectors and the predicted values of the target scattering amplitudes are scattering model-dependent (see Figs. 3 and 4). In this the effect of scattering model is significant, particularly for targets in close proximity, as expected (see Fig. 4).

ACKNOWLEDGMENT

[1] M. Fink, D. Cassereau, A. Derode, C. Prada, P. Roux, M. Tanter, J. L. Thomas, and F. Wu, "Time-reversed acoustics," Rep. Prog. Phys. **63**, 1933–1995 (2000).

[2] G. Montaldo, P. Roux, A. Derode, C. Negreira, and M. Fink, "Generation of very high pressure pulses with 1-bit time reversal in a solid waveguide," J. Acoust. Soc. Am. **110**, 2849–2857 (2001).

[3] J. S. Kim and K. C. Shin, "Multiple focusing with adaptive time-reversal mirror," J. Acoust. Soc. Am. **115**, 600–606 (2004).

[4] A. Derode, A. Tourin, J. de Rosny, M. Tanter, S. Yon, and M. Fink,

Gruber *et al.*: Time-reversal imaging

"Taking advantage of multiple scattering to communicate with time-reversal antennas," Phys. Rev. Lett. **90**, 014301 (2003).

[5] D. M. Fromm, C. F. Gaumond, J. F. Lingevitch, R. C. Gauss, and R. Menis, "Detection in shallow water using broadband-DORT," J. Acoust. Soc. Am. **114**, 2399 (2003).

[6] L. Carin, H. Liu, T. Yoder, L. Couchman, B. Houston, and J. Bucaro, "Wideband time-reversal imaging of an elastic target in an acoustic waveguide," J. Acoust. Soc. Am. **115**, 259–268 (2004).

[7] H. Lev-Ari and A. J. Devaney, "The time-reversal technique re-interpreted: Subspace-based signal processing for multi-static target location," IEEE Sensor Array and Multichannel Signal Processing Workshop, Cambridge, MA, 2000, pp. 509–513.

[8] S. K. Lehman and A. J. Devaney, "Transmission mode time-reversal super-resolution imaging," J. Acoust. Soc. Am. **113**, 2742–2753 (2003).

[9] C. Prada and J. L. Thomas, "Experimental subwavelength localization of scatterers by decomposition of the time reversal operator interpreted as a covariance matrix," J. Acoust. Soc. Am. **114**, 235–243 (2003).

[10] C. Prada, J. L. Thomas, and M. Fink, "The iterative time reversal process: Analysis of the convergence," J. Acoust. Soc. Am. **97**, 62–71 (1995).

[11] C. Prada, S. Manneville, D. Spoliansky, and M. Fink, "Decomposition of the time reversal operator: Detection and selective focusing on two scatterers," J. Acoust. Soc. Am. **99**, 2067–2076 (1996).

[12] L. Borcea, G. Papanicolaou, C. Tsogka, and J. Berryman, "Imaging and time reversal in random media," Inverse Probl. **18**, 1247–1279 (2002).

J. Acoust. Soc. Am., Vol. 115, No. 6, June 2004

Gruber *et al.*: Time-reversal imaging   3047